Supplementary information for:

Epitaxial growth and enhanced conductivity of an IT-SOFC cathode based on a complex perovskite superstructure with six distinct cation sites

R. Sayers[(a)], N.L.O. Flack[(a)], J. Alaria[(a)], P. A. Chater[(a)], R. G. Palgrave[(a)], S.R.C. McMitchell[(a)], S. Romani[(b)], Q.M. Ramasse[(c)], T. J. Pennycook[(c,d)], M.J. Rosseinsky*[(a)]

(a) Department of Chemistry, University of Liverpool, Liverpool, L69 7ZD
(b) Nanoinvestigation Centre at Liverpool (NiCaL), Department of Materials & Structures, The University of Liverpool, Waterhouse Building, Block C, 1-3 Brownlow Street, Liverpool, L69 3GL
(c) SuperSTEM Laboratory, STFC Daresbury Campus, Keckwick Lane, Daresbury WA4 4AD, U.K.
(d) Department of Materials, University of Oxford, Parks Road, Oxford OX1 3PH, U.K.

1) Thin film optimisation: XRD

Standard θ/2θ XRD pattern collected on films prepared under 1 mTorr of oxygen with varying growth temperature using a Panalytical X'Pert Pro diffractometer equipped with a Cu tube and a Pixcel detector are presented in Fig. S1 (a). Several competing phases are present in the film and only at 850 ^{o}C does the 10 a_p phase form. Standard θ/2θ XRD patterns were collected on films prepared with different fluences at 850 ^{o}C using a Panalytical X'Pert Pro diffractometer equipped with a monochromated Co tube and a Xcelerator detector are presented in Fig. S1 (b). To avoid the formation of the competing 3 a_p phase, a growth temperature of 850 ^{o}C and a fluence of 0.27 Jcm^{-2} is used.

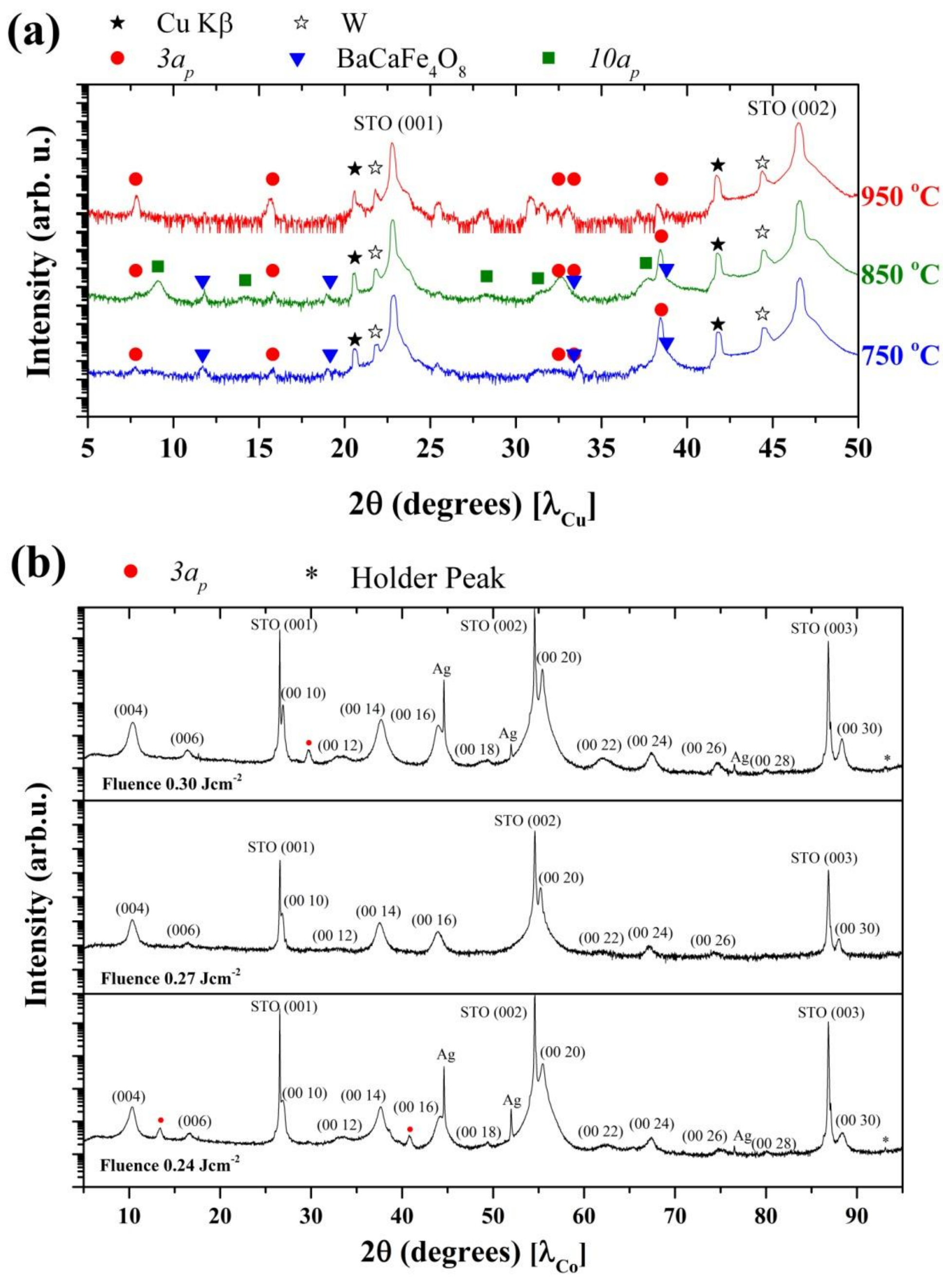

Fig. S1 (a) XRD patterns of the optimization of the 10 a_p growth showing the effect the growth temperature has on the film. The radiation used to collect the patterns was contaminated by Cu K_β and W components marked with asterisks. (b) XRD patterns showing the effect of fluence on the formation of the 3 a_p phase. The silver peaks that are present are a result of the silver DAG that was used to stick the substrates to the heater block.

Table S1 Simulated peak intensities for the 10 a_p material. Bold values in the cells are not observed in the 10 a_p XRD pattern due to their low intensity. Italicized values in red show that the expected intensities of the (0 2 20) and (2 0 20) peaks (relevant for the off-axis scans) are very similar.

h	k	l	d (Å)	2θ (degrees)	Normalised IIp
0	0	2	19.10085	4.62250	100
0	0	4	9.55043	9.25253	71.51099
0	**0**	**6**	**6.36695**	**13.89777**	**2.625543**
0	**0**	**8**	**4.77521**	**18.56609**	**0.26659**
0	0	10	3.82017	23.26572	3.648396
0	0	12	3.18348	28.00540	4.78733
0	0	14	2.72869	32.79452	17.53466
0	0	16	2.38761	37.64332	9.550011
0	**0**	**18**	**2.12232**	**42.56314**	**0.304649**
0	0	20	1.91008	47.56671	67.484
0	0	22	1.73644	52.66855	0.641703
0	0	24	1.59174	57.88548	0.511366
0	***2***	***20***	***1.57282***	***58.64924***	***46.64372***
2	***0***	***20***	***1.56847***	***58.82777***	***48.67444***
0	0	26	1.46930	63.23732	0.103495
0	**0**	**28**	**1.36435**	**68.74782**	**0.110526**
0	0	30	1.27339	74.44605	0.476983

2) Simulated pole figures

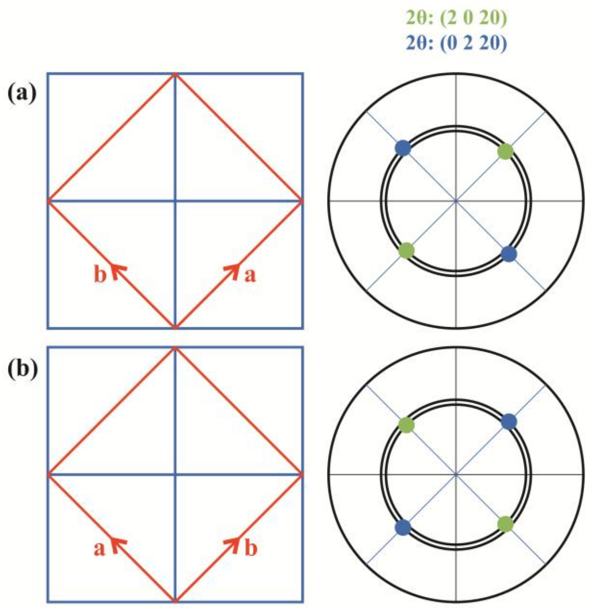

Fig. S2 Schematic showing the layer orientation on the substrate and the expected pole figures for the two Bragg reflections considered in the main text.

3) Additional TEM images

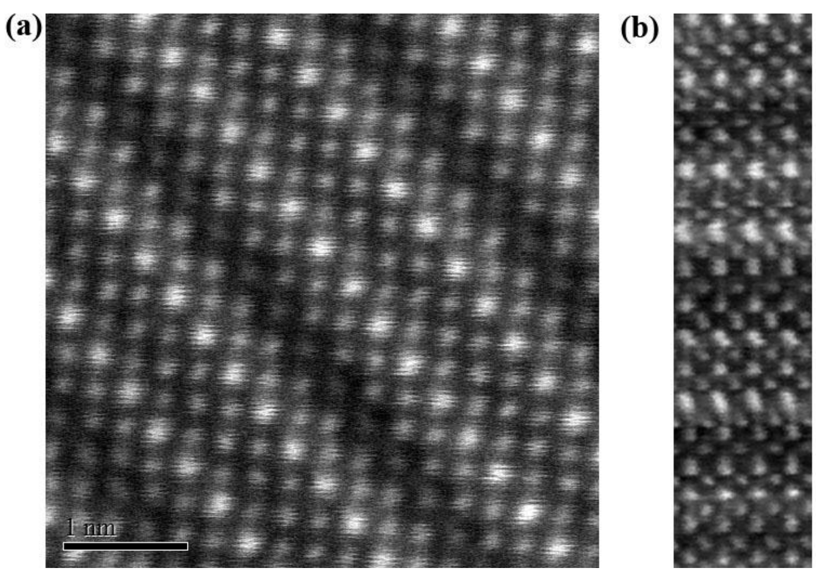

Fig. S3 (a) Unfiltered HAADF STEM image used in Fig. 8(a), (b) HAADF signal recorded simultaneously with EELS spectra presented in Fig. 9(b)-(e).

4) Thermal stability of the thin film

To study the thermal stability of the film a sample was heated to 600 ^{o}C at a heating rate of 3 ^{o}min^{-1}; once the film reached 600 ^{o}C it dwelled at temperature for 200 hours. The X-ray diffraction pattern of the film was then remeasured (Fig. S4).

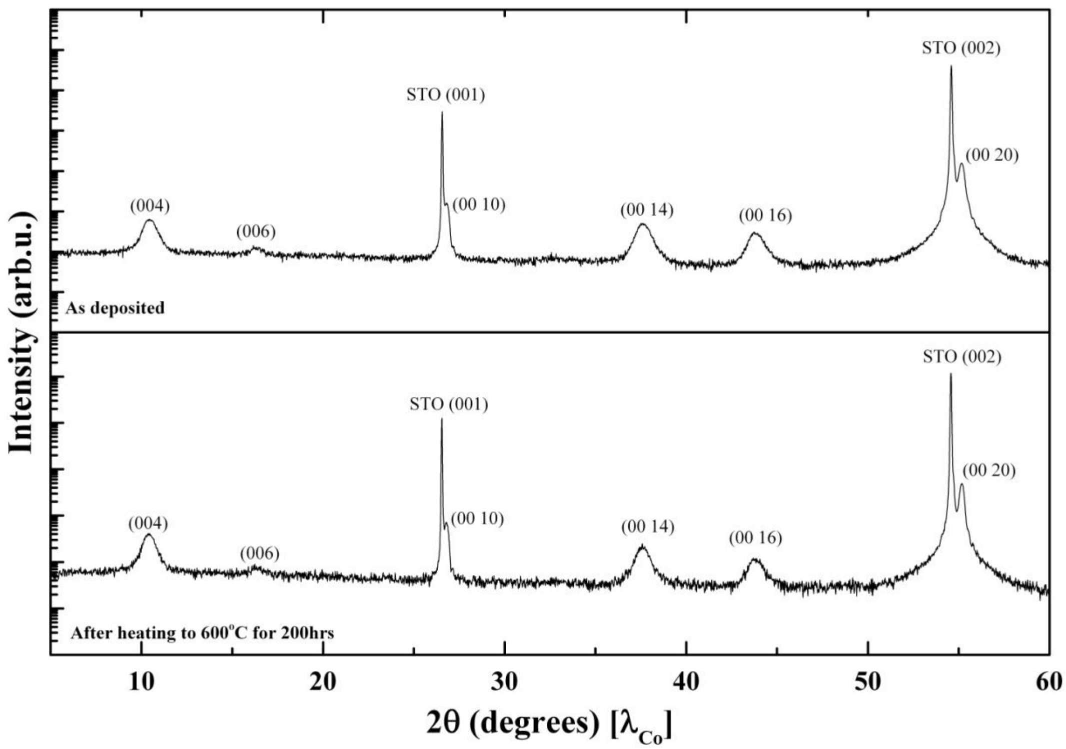

Fig. S4 XRD patterns of the 10 a_p film before and after annealing to 600 ^{o}C for 200 hrs.

No additional peaks are present in the XRD pattern after 200 hours, indicating good thermal stability at IT-SOFC operating temperatures.

AC-impedance was measured on 3 full thermal cycles and the extracted total conductivity is presented on Fig. S5 (a). A good reproducibility is observed as highlighted in Table S2 with similar values of the conductivity measured at 550 ^{o}C for all cooling cycles.

Table S2 Total conductivity at 550 ^{o}C for each cooling cycle.

	Cycle 1	Repeat Cycle 1	Repeat Cycle 2	Repeat Cycle 3
Conductivity (S.cm^{-1}) at 550^{o}C	27.5	26.0	26.3	26.1

The phase stability after these measurement cycles was confirmed by XRD. The only additional peaks present in the θ/2θ pattern shown in Fig. S5 (c) are those of the gold electrodes. This indicates that the 10 a_p film is stable after heating and cooling cycles to 600 ^{o}C. Further evidence of the structural stability is presented on Fig. S5 (b) where the lattice parameter of the 10 a_p only changes by 0.08 % which could be due to a slight change in oxygen stoichiometry.

From the combined information reported in Fig. S5 and Table S2, it can be clearly seen that the cycles were very reproducible. This also suggests that the 10 a_p film has a good level of durability as each cycle has a run time of approximately 77 hours.

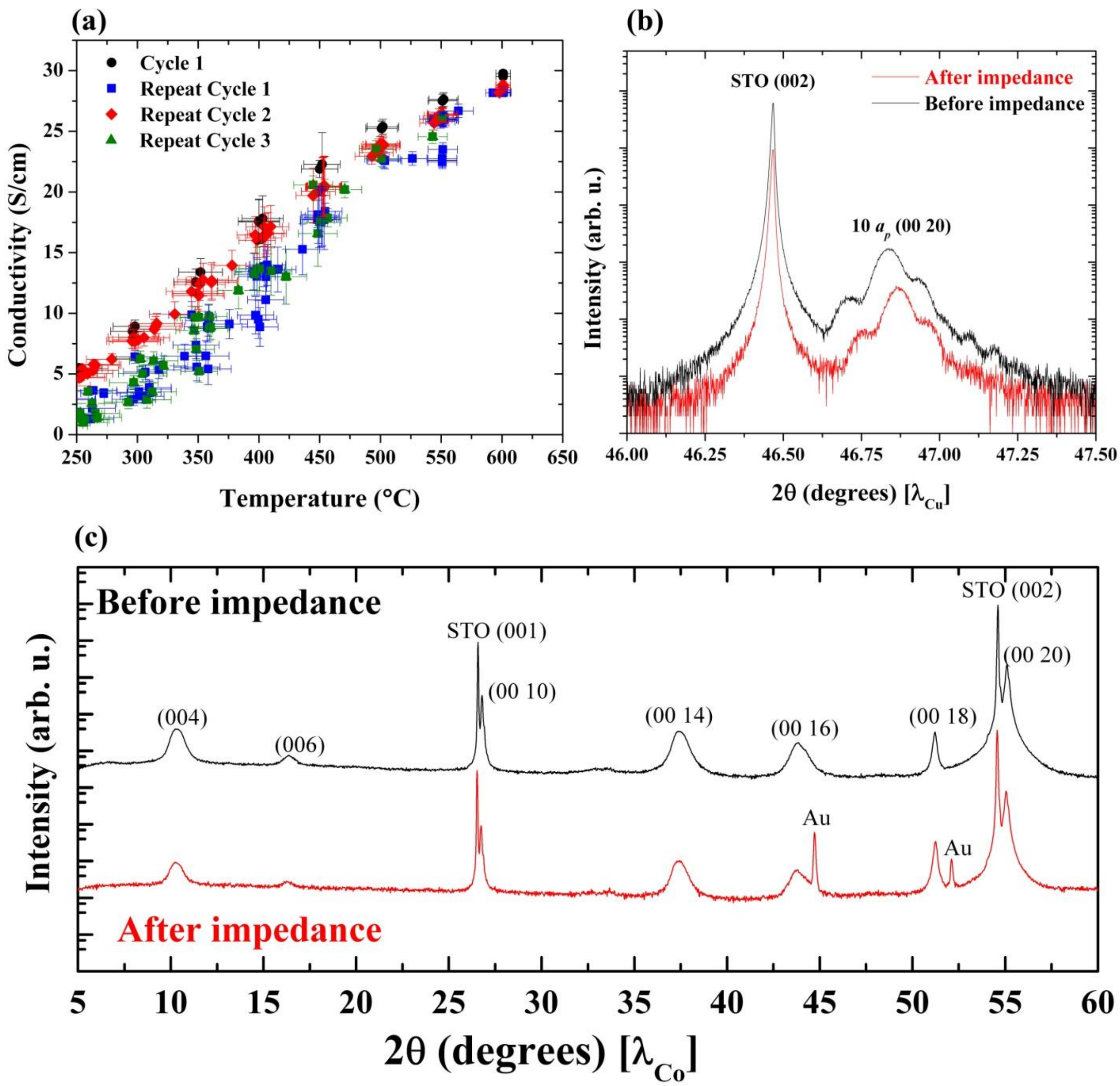

Fig. S5 (a) AC impedance cooling cycles measured on the 10 a_p film, showing the reproducibility and the durability of the film. (b) HRXRD around the (00 20) peak (c) XRD patterns before and after AC impedance measurements to 600 °C.

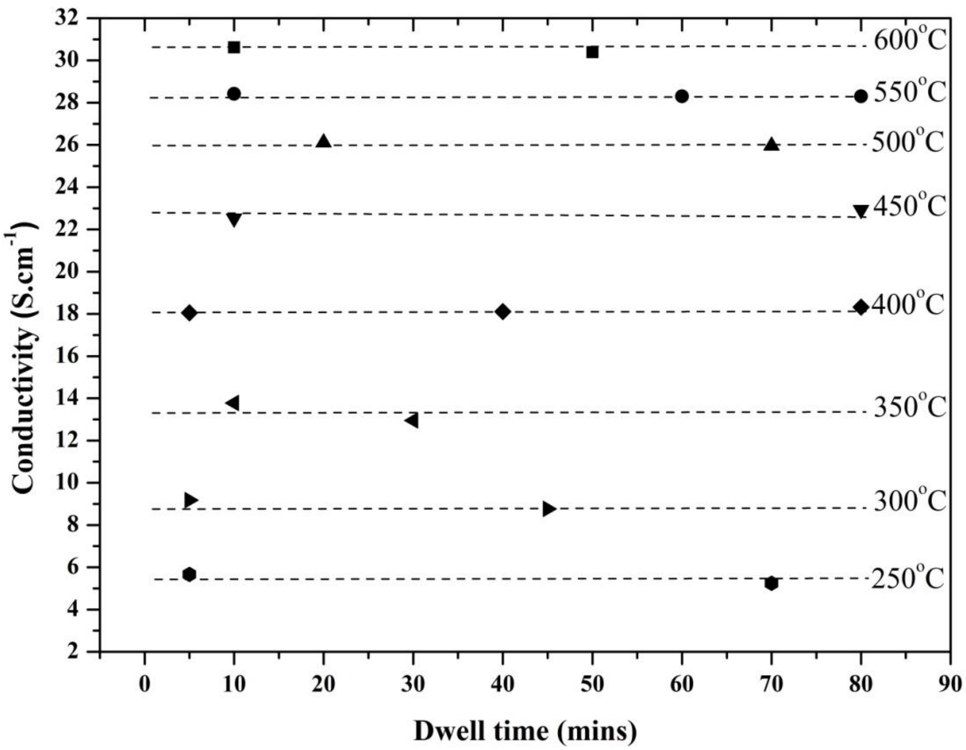

Fig. S6 Conductivity values as a function of dwell time from AC impedance of thin film on cooling in Cycle 1; the dashed lines are linear extrapolations. It can be seen that there is no significant change in the conductivity on cooling as a function of time at constant temperature.